NUCLEAR THEORY, Vol. 34 (2015)
eds. M. Gaidarov, N. Minkov, Heron Press, Sofia

Inelastic Scattering of Protons on ^{9}Be Nucleus ($J^\pi = 3/2^+, 5/2^-$) in the Glauber Theory

M.A. Zhusupov[1], **E.T. Ibraeva**[2], **R.S. Kabatayeva**[1]

[1]Al-Farabi Kazakh National University, Almaty, Kazakhstan

[2]Institute of Nuclear Physics, Almaty, Kazakhstan

Abstract. In the present paper the authors have calculated the differential cross sections of inelastic scattering of protons on the excited states of ^{9}Be nucleus in the framework of the Glauber diffraction theory of multiple scattering. The ^{9}Be nucleus was considered in the three-particle $2\alpha n$-model, wave functions of which were calculated with different potentials of pair interactions. The excited states of ^{9}Be nucleus reveal the halo-structure what defines the behavior of the cross sections in all angle range. The calculated results are compared with experimental data and results of other authors.

1 Introduction

The new challenge for study of the weakly-bound nuclei is the discovery of the exotic structure (halo and skin) of the number of unstable neutron- and proton-rich isotopes. The ^{9}Be nucleus is a stable strongly deformed one (quadrupole moment Q = 52.88(38) mb [1]), weakly-bound in the cluster channel $^9\text{Be} \to \alpha + \alpha + n$ ($\epsilon = 1.57$ MeV) [1], that is the direct indication to its three-particle $\alpha + \alpha + n$ structure. This nucleus can be considered as borromean one since in the framework of the three-particle $\alpha + \alpha + n$ picture in ^{9}Be nucleus there are not two components able to form the bound system. A consideration of this nucleus in the three-particle model led to a better understanding of the halo and the molecular structure of three-particle systems [2]. Besides the channel of three-particle disintegration the ^{9}Be nucleus can decay by the two-particle channels $^9\text{Be} \to n + {}^8\text{Be}$ or $^9\text{Be} \to \alpha + {}^5\text{He}$. It is shown in [3], that the ^{8}Be + n cluster structure only of the ^{9}Be nucleus explains the data on ^{9}Be + ^{208}Pb scattering adequately. In the recent high precision experiment [4] on measurement of cross section of elastic ^{9}Be + ^{208}Pb scattering at the sub-barrier energies it is shown that the deviation observed in cross section from Rutherford scattering indicates to the dominating ^{8}Be + n cluster structure of ^{9}Be nucleus while α + ^{5}He structure is represented less clearly. The positive-parity states reproduce better the ^{8}Be + n structure [5], while concerning the negative-parity states and the importance of the α + ^{5}He structure for them there is some uncertainty. It is shown in [6] and [7], that the dynamic evolution from the α + ^{5}He structure at small

distances to the n + ^{8}Be structure at large distances describes better the levels with quantum numbers $1/2^+$ and $5/2^-$.

The elastic and inelastic (for the level $J^\pi = 5/2^-$, $E^* = 2.44$ MeV) scattering of the polarized protons at energy of 220 MeV have been earlier measured in [8]. A calculation of the differential cross section, analyzing power and depolarization were carried out in the optical model, in the DWIA and in the coupled channels method using the spherical Wood-Saxon potential. It is shown that the simple optical model and the first approximation of the DWIA describe the cross section and the polarizing characteristics less well than the coupled channels method.

The differential cross sections and the analyzing powers of the p^9Be scattering and charge-exchange ^{9}Be(p, n)^{9}B reactions at $E = 180$ MeV to the ground and the excited states of the ^{9}Be nucleus were calculated in the distorted waves approximation using the effective interaction dependent on the density and based on the Paris potential [9]. A comparison with the experimental data showed that with account of the quadrupole deformation of the ^{9}Be nucleus the differential cross sections are well reproduced for both the ground and the excited states of negative parity in the wide range of the momentum transfer $q = 0 \div 3$ fm^{-1} while for the positive-parity states the situation is worse.

A study of the inelastic scattering of α-particles on ^{9}Be nucleus and reactions of one-particle transfer ^{9}Be(α, ^{3}He)^{10}Be and ^{9}Be(α, t)^{10}B has been recently carried out in Finland (Cyclotron Facility of the Accelerator Laboratory, Jyvaskayla University) at $E_\alpha = 63$ MeV. The measured differential cross sections for the ground and several low-lying ($5/2^-$, $7/2^-$, $9/2^-$) states were analyzed in the framework of the optical model, the coupled channels method and the DWBA [10]. In many works the special attention was given to the role of the extra valence nucleons and their influence on the cluster structure of the excited states. As the authors emphasize [11], "observation of halos in the excited states can drastically extend the existing knowledge about exotic states of nuclei, since some new features of nuclear structure might become apparent".

The present work is the continuation of the previous ones [12–14], where the elastic and inelastic (for the $J^\pi = 1/2^+$ level) differential cross sections in the framework of the Glauber theory were calculated at $E = 180$ MeV and 220 MeV and compared to the experimental data [8, 9]. In paper [14] there is a calculation of the mean-square radii of the ground state (2.45 fm) and the $1/2^+$ state (2.83 fm). In the above-mentioned excited state the ^{9}Be nucleus has more extended, diffuse structure in comparison with the wave function of the ground state, and as a result it was concluded that this level is a halo state. The goal of this work is a calculation of the differential cross section of the inelastic scattering of protons with energy of 180 MeV to the excited $3/2^+$ and $5/2^-$ states of the ^{9}Be nucleus in the framework of the Glauber theory and a comparison with the results obtained in other formalisms.

2 Brief Formalism

The matrix element of scattering in the Glauber theory is the following [15]:

$$M_{if}(\vec{q}) = \sum_{M_J, M'_J} \frac{ik}{2\pi} \int d^2\vec{\rho} e^{i\vec{q}\vec{\rho}} \delta(\vec{R}_A) \langle \Psi_f^{J'M'_J} |\Omega| \Psi_i^{JM_J} \rangle, \qquad (1)$$

where $\vec{\rho}$ is an impact parameter, which is a two-dimensional vector in the Glauber theory, $\vec{R_A}$ is the coordinate of the target nucleus mass center, $\Psi_i^{JM_J}$, $\Psi_f^{J'M'_J}$ – initial and final states wave functions of the target nucleus, $\vec{k}$, $\vec{k'}$ are incoming and outgoing momenta of the proton, $\vec{q}$ is the momentum transfer in the reaction $\vec{q} = \vec{k} - \vec{k'}$.

The wave function of the ^{9}Be nucleus in $2\alpha n$-model [16, 17] with total angular momentum J and its projection M_J is written as follows:

$$\Psi_{i,f}^{JM_J} = \varphi_1(\xi_{1-4})\varphi_2(\xi_{5-8}) \sum_L \Psi_L^{JM_J}(\vec{r}, \vec{R}), \qquad (2)$$

where $\varphi_1(\xi_{1-4}), \varphi_2(\xi_{5-8})$ are the wave functions of the α-particles dependent on the internal coordinates of the system of four nucleons, $\Psi_L^{JM_J}(\vec{r},\vec{R})$ is a function of relative motion in terms of the Jacobi coordinates. The wave function $\Psi_L^{JM_J}(\vec{r},\vec{R})$ is expanded by the partial waves

$$\Psi_L^{JM_J}(\vec{r}, \vec{R}) = \sum_{M_L M_S m\mu} \langle LM_L SM_S | JM_J \rangle \langle \lambda\mu\ell m | LM_L \rangle r^\lambda Y_{\lambda\mu}(\Omega_r) \times R^\ell Y_{\ell m}(\Omega_R) \chi_{SM_S} \sum_{ij} C_{ij}^{\lambda\ell} \exp(-\alpha_i r^2 - \beta_j R^2), \qquad (3)$$

where $\langle LM_L SM_S | JM_J \rangle$, $\langle \lambda\mu\ell m | LM_L \rangle$ are the Clebsch-Gordan coefficients determining the scheme of momenta addition, $Y_{\lambda\mu}(\Omega_r)$, $Y_{\ell m}(\Omega_R)$ are the spherical functions, $\chi_{SM_S} = \chi_{\frac{1}{2}m_N}\varphi_1(\xi_{1-4})\varphi_2(\xi_{5-8})$ – spin function of the valence nucleon and the α-particle, $C_{ij}^{\lambda\ell}$, α_j, β_j are the linear and nonlinear variation parameters. The weight of the three configurations of the wave function and some static characteristics of the ^{9}Be nucleus are represented in paper [16].

In the ground ($J^\pi = 3/2^-$) state the three components contribute with about the same weights with quantum numbers ($\lambda\ell L$) = (011), (211), (212). The excited states $J^\pi = 3/2^-$ ($E^* = 4.704$ MeV with weight of 99.5%) and $J^\pi = 5/2^-$ ($E^* = 2.43$ MeV with weight of 97.5%) contain one dominating component $(\lambda\ell L) = (022)$ and $(\lambda\ell L) = (212)$ [16], respectively.

Let's write the matrix element (1) after substitution of the wave function (3)

$$M_{if}(\vec{q}) = \frac{ik}{2\pi} \sum_{M_L, M'_L, \mu, \mu'} \langle LM_L SM_S | JM_J \rangle \langle L'M'_L S'M'_S | J'M'_J \rangle$$
$$\times \langle \lambda\mu\ell m | LM_L \rangle \langle \lambda'\mu'\ell'm' | L'M'_L \rangle$$
$$\times \sum_{iji'j'} C_{ij}^{\lambda\ell} C_{i'j'}^{\lambda'\ell'} \int d^2\rho e^{i\vec{q}\vec{\rho}} \Big\langle r^\lambda Y_{\lambda\mu}(\Omega_r) R^\ell Y_{\ell m}(\Omega_R)$$
$$\times e^{(-\alpha_i r^2 - \beta_j R^2)} \, |\Omega| \, r^{\lambda'} Y_{\lambda'\mu'}(\Omega_r) R^{\ell'} Y_{\ell'm'}(\Omega_R) e^{(-\alpha'_i r^2 - \beta'_j R^2)} \Big\rangle. \quad (4)$$

The general form of the Glauber multiple scattering operator is written as alternating-sign series of one-, two-, ..., A-fold (where A is the number of nucleons in the target nucleus) collisions of the incident proton with the nucleons of the nucleus [15]

$$\Omega = 1 - \prod_{j=1}^{A} (1 - \omega_j(\vec{\rho} - \vec{\rho_j}))$$
$$= \sum_{j=1}^{A} \omega_j + \sum_{j<\mu} \omega_j \omega_\mu - \sum_{j<\mu<\eta} \omega_j \omega_\mu \omega_\eta + \cdots + (-1)^{A-1} \omega_1 \omega_2 \ldots \omega_A, \quad (5)$$

where ω_j - is a profile function dependent on the elementary $f_{xj}(q)$-amplitude

$$\omega_j(\vec{\rho} - \vec{\rho_j}) = \frac{1}{2\pi ik} \int d^2\vec{q} \exp[-i\vec{q}(\vec{\rho} - \vec{\rho_j})] f_{xN}(q), \quad (6)$$

where $x = (n, \alpha)$. The elementary amplitude is parametrized in the following standard way:

$$f_{xN} = \frac{k\sigma_{xN}}{4\pi}(i + \epsilon_{xN}) exp(-\beta_{xN} q^2/2), \quad (7)$$

where σ_{xN} is the total cross section of scattering on a nucleon, ϵ_{xN} is the ratio of the real part of the amplitude to the imaginary one, β_{xN} is the slope parameter of the amplitude cone. The parameters at different energies are provided in paper [12].

Substituting the wave function of the ^{9}Be nucleus in $2\alpha n$-model into the matrix element, it is convenient to transform the Ω operator to a form conjugated to this model, considering collisions not with separate nucleons, but with α-particle clusters as structureless and the nucleon. In accordance with this approach the series of multiple scattering (5) for the ^{9}Be nucleus is rewritten as follows:

$$\Omega = \sum_{j=1}^{3} \omega_j - \sum_{i<j=1}^{3} \omega_i \omega_j + \omega_{\alpha_1} \omega_{\alpha_2} \omega_n, \quad (8)$$

where $j = 1, 2$ enumerate α_1 and α_2, $j = 3$ enumerates the nucleon.

After substitution of the elementary amplitude (7) into the profile function (6) and integration with respect to $\vec{q}$ variable, one gets

$$\omega_j(\vec{\rho}-\vec{\rho_j}) = F_j exp[-(\vec{\rho}-\vec{\rho_j})^2\eta_j], \tag{9}$$

where

$$F_j = \frac{\sigma_{xj}}{4\pi\beta_{xj}}(i+\epsilon_{xj}), \qquad \eta_j = \frac{1}{2\beta_{xj}}. \tag{10}$$

For further calculations it is necessary to change from single-particle $\{\vec{\rho_1},\vec{\rho_2},\vec{\rho_3}\}$ coordinates of nucleons in the Ω operator to the Jacobi coordinates $\{\vec{r},\vec{R}\}$ and the coordinate of the ^{9}Be nucleus mass center $\vec{R_9}$

$$\vec{r} = \vec{\rho_1}-\vec{\rho_2}, \qquad \vec{R} = \frac{1}{2}(\vec{\rho_1}+\vec{\rho_2})-\vec{\rho_3}, \qquad \vec{R_9} = \frac{1}{9}(4\vec{\rho_1}+4\vec{\rho_2}+\vec{\rho_3}). \tag{11}$$

As it was shown in works [13, 14] after some transformations the Ω operator in the Jacobi coordinates can be written as follows:

$$\Omega = (\vec{G}\vec{H}) = \sum_{k=1}^{7} G_k H_k, \tag{12}$$

where the summation over k index means a summation over scattering order: $k = 1 \div 3$ – single collisions, $k = 4 \div 6$ – double collisions, $k = 7$ – triple collisions. Here $\vec{G}$ is a 7-dimensional vector with components

$$\begin{aligned}\vec{G} &= (G_1, G_2, \ldots, G_7) \\ &= (F_\alpha, F_\alpha, F_n, -F_\alpha F_\alpha, -F_\alpha F_n, -F_\alpha F_n, F_\alpha F_\alpha F_n).\end{aligned} \tag{13}$$

The components of the vector $\vec{H} = (H_1, H_2, H_3)$ are expressed through the exponential function of coordinates in a form

$$H_k = \exp(-a_k\vec{\rho_\perp}^{\,2} - b_k\vec{R_\perp}^{\,2} - c_k\vec{r_\perp}^{\,2} + d_k\vec{\rho_\perp}\vec{R_\perp} + l_k\vec{\rho_\perp}\vec{r_\perp} + f_k\vec{R_\perp}\vec{r_\perp}), \tag{14}$$

where

$$\begin{aligned}
a_k &= (\eta_\alpha, \eta_\alpha, \eta_n, 2\eta_\alpha, (\eta_\alpha+\eta_n), (\eta_\alpha+\eta_n), (2\eta_\alpha+\eta_n)), \\
b_k &= \frac{1}{81}(\eta_\alpha, \eta_\alpha, 64\eta_n, 2\eta_\alpha, (\eta_\alpha+64\eta_n), (\eta_\alpha+64\eta_n), (2\eta_\alpha+64\eta_n)), \\
c_k &= \frac{1}{2}(\frac{\eta_\alpha}{2}, \frac{\eta_\alpha}{2}, 0, \eta_\alpha, \frac{\eta_\alpha}{2}, \frac{\eta_\alpha}{2}, \eta_\alpha), \\
d_m^c &= \frac{2}{9}(\eta_\alpha, \eta_\alpha, 8\eta_n, 2\eta_\alpha, (2\eta_\alpha+8\eta_n), (2\eta_\alpha+8\eta_n), (2\eta_\alpha+8\eta_n)), \\
l_m^c &= (-\eta_\alpha, \eta_\alpha, 0, 0, -\eta_\alpha, \eta_\alpha, 0), \\
f_m^c &= \frac{1}{9}(\eta_\alpha, -\eta_\alpha, 0, 0, \eta_\alpha, -\eta_\alpha, 0),
\end{aligned}$$

where coefficients $a_k, b_k, ...$ are defined with the formulas (10).

Substituting the operator (12) into the formula (4), the matrix element can be written in a form:

$$M_{if}^{(\lambda\ell L)}(q) = \frac{ik}{2\pi}\sum_{k=1}^{7}\sum_{iji'j'}\sum_{L\lambda L'\lambda'} G_k C_{ij}^{\lambda\ell} C_{i'j'}^{\lambda'\ell'}$$
$$\times \int \tilde{H}_k(\rho_\perp, r_\perp, R_\perp, q) H_{k_z}(r_z, R_z) Q_{L'S'\lambda'\ell'}^{LS\lambda\ell}(r^\lambda, R^\ell) d^2\rho d\vec{r} d\vec{R}, \quad (15)$$

where the following notations are introduced

$$Q_{L'S'\lambda'\ell'}^{LS\lambda\ell}(r^\lambda, R^\ell) = \sum_{M_L M'_L \mu\mu'} \langle LM_L SM_S|JM_J\rangle \langle L'M'_L S'M'_S|J'M'_J\rangle$$
$$\times \langle \lambda\mu\ell m|LM_L\rangle \langle \lambda'\mu'\ell'm'|L'M'_L\rangle$$
$$\times \langle r^\lambda Y_{\lambda\mu}(r)|r^{\lambda'} Y_{\lambda'\mu'}(r)\rangle \langle R^\ell Y_{\ell m}|R^{\ell'} Y_{\ell' m'}\rangle, \quad (16)$$
$$\tilde{H}_k(\rho_\perp, r_\perp, R_\perp, q) = \exp(-a_k\rho^2 - \tilde{b_k} R_\perp^2 - \tilde{c_k} r_\perp^2$$
$$+ d_k \rho_\perp R_\perp + \ell_k \rho_\perp r_\perp + f_k R_\perp r_\perp + i\vec{q}\vec{\rho}), \quad (17)$$
$$\tilde{b_k} = b_k + \beta_j + \beta'_j, \qquad \tilde{c_k} = c_k + \alpha_i + \alpha'_i, \quad (18)$$
$$H_z(r_z, R_z) = \exp(-(\alpha_i + \alpha'_i) r_z^2 - (\beta_j + \beta'_j) R_z^2). \quad (19)$$

In the polynomial $Q_{L'S'\lambda'\ell'}^{LS\lambda\ell}$ there is a summation of the Clebsch-Gordan coefficients with the spherical functions (regular sectorial harmonics), which in Cartesian coordinates are represented with harmonic polynomials by x, y, z [18]

$$r^\ell Y_{\ell m}(\Omega_r) = \sqrt{\frac{2\ell+1}{4\pi}(\ell+m)!(\ell-m)!}$$
$$\times \sum_{pnt} \frac{1}{p!n!t!}(-\frac{x+iy}{2})^p (\frac{x-iy}{2})^n z^t, \quad (20)$$

where $p + n + t = \ell$, $p - n = m$, and p, n, t are integer positive numbers.

The polynomial $Q_{L'S'\lambda'\ell'}^{LS\lambda\ell}$ is written as the product

$$Q_{L'S'\lambda'\ell'}^{LS\lambda\ell}(r^\lambda, R^\ell) = \sum_{M_L M'_L M_S M'_S} \langle LM_L SM_S|JM_J\rangle \langle L'M'_L S'M'_S|J'M'_J\rangle$$
$$\times \sum_{\lambda\mu\lambda'\mu'\ell m\ell' m'} \langle \lambda\mu\ell m|LM_L\rangle \langle \lambda'\mu'\ell'm'|L'M'_L\rangle K_{\lambda\mu}(r^\lambda) K_{\ell m}(R^\ell), \quad (21)$$

where

$$K_{\lambda\mu}(r^\lambda) = \langle r^\lambda Y_{\lambda\mu}|r^\lambda Y_{\lambda\mu'}\rangle, \qquad K_{\ell m}(R^\ell) = \langle R^\ell Y_{\ell m}|R^\ell Y_{\ell m'}\rangle.$$

Let's calculate the quantities $K_{\lambda\mu}(r^\lambda)$, $K_{\ell m}(R^\ell)$ for quantum numbers $\ell = 1$ and $\lambda = 2$ for the level $J^\pi = 5/2^-$. The calculations for the level $J^\pi = 3/2^+$ are presented in the work [13].

$$K_{1m}(R) = \langle RY_{1m}|RY_{1m'}\rangle$$
$$= (D1)^2\Big\{R^2_{x+y}\delta_{m1}\delta_{m'1} + R^2_{x-y}\delta_{m-1}\delta_{m'-1}$$
$$+ 2R_{x^2+y^2}\delta_{m1}\delta_{m'-1}\Big\}, \quad (22)$$

where $D1 = \frac{1}{2}\sqrt{\frac{3}{2\pi}}$, $R_{x+y} = -(R_x + iR_y)$, $R_{x-y} = (R_x - iR_y)$.

$$K_{2\mu}(r^2) = \langle r^2Y_{2\mu}|r^2Y_{2\mu'}\rangle$$
$$= (D2)^2\{\tilde{r}^2_{xyz}\delta_{\mu 0}(r^2_{xyz}\delta_{\mu'0} + r^2_{x+y}[\delta_{\mu 2} + \delta_{\mu' 2}]$$
$$+ r^2_{x-y}[\delta_{\mu -2} + \delta_{\mu' -2}]) + r^2_{x+y}\delta_{\mu 2}\delta_{\mu' 2}$$
$$+ r^4_{x-y}\delta_{\mu -2}\delta_{\mu' -2} + 2r^2_{x+y}r^2_{x-y}\delta_{\mu 2}\delta_{\mu' -2}\}, \quad (23)$$

where

$$D2 = \frac{1}{8}\sqrt{\frac{30}{\pi}}, \qquad r_{x+y} = -(r_x + ir_y),$$
$$r_{x-y} = (r_x - ir_y), \qquad r^2_{xyz} = 2r^2_z - r^2_x - r^2_y.$$

Further calculation of the $Q^{LS\lambda\ell}_{L'S'\lambda'\ell'}$ polynomials and the $M^{(\lambda\ell L)}_{if}$ matrix element was carried out using the MAPLE program.

The differential cross section is a square of the matrix element module

$$\frac{d\sigma}{d\Omega} = \frac{1}{2J+1}\sum_{M_J M'_J}|M_{if}(\vec{q})|^2. \quad (24)$$

3 Wave Functions of ^{9}Be in 2αn Model

The calculation of the wave function in $2\alpha n$ model [16, 17] was carried out in the variation stochastic method with three couple interactions $V_{\alpha\alpha}$, $V_{\alpha_1 n}$, $V_{\alpha_2 n}$.

Model 1 : $V_{\alpha\alpha}$ is the Ali-Bodmer potential (AB) [19], shallow one with repulsive core at small distances, not containing the forbidden states;

Model 2 : $V_{\alpha\alpha}$ is the Buck potential (B) [20], deep attractive one with the forbidden states, describing scattering phases with $\lambda = 0, 2, 4, 6$; $V_{\alpha n}$ is the same as in model 1.

In both models $V_{\alpha n}$ was used – a potential with exchange Majorana component which leads to the even-odd splitting of the phase shifts.

Let's move to a consideration of the geometric structure of the wave function which allows one to visualize the relative location of clusters and understand the manifestation of their features in the scattering process.

What is the difference between wave functions calculated with different potentials? As it is shown in works [16, 17] in the ground state the wave function in the model 1 due to presence of the repulsive core inside the nucleus is

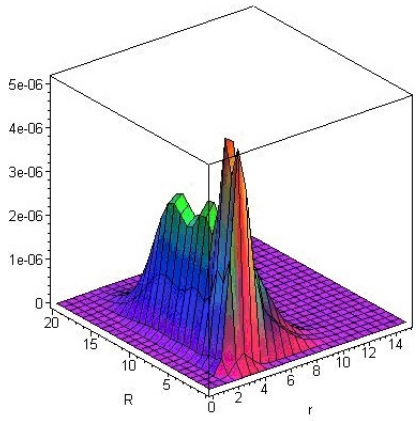

Figure 1. Three-dimensional profile of the ^{9}Be nucleus wave function in the excited $J^\pi = 3/2^+$ state with AB potential

close to zero ("disappear"), and it reaches the maximal value on the periphery at $r > 3 \div 4$ fm. In the model 2 the wave function is more strongly involved into the nucleus, and there are a node and two maximums inside. Let's see what are the wave functions like in the excited states?

In Figures 1 and 2 there are behaviors of three-dimensional profiles of the wave functions $W(r, R) = \sum_{\lambda \ell L} |\Psi^{\lambda \ell L}|^2 r^2 R^2$ in the excited $J^\pi = 3/2^+, 5/2^-$ states.

In Figure 1 there is a three-dimensional profile of the wave function of the excited $J^\pi = 3/2^+$ state calculated with AB potential. One can see in the figure that the wave function inside the nucleus equals zero ($r \leq 1.5$ fm), reaches the maximal value at $(r, R) = (3.5, 3.2)$ fm, decreases very slowly, oscillating, and asymptotically approaches zero at $(r, R) = (10.0, 18.0)$ fm. If there is a large r-coordinate extension of the wave function in the ground state [16, 17], then in the $J^\pi = 3/2^+$ state, in opposite, the large R-coordinate extension is observed. The minor first peak at R = 0.5 fm demonstrates the contribution of the cigar-shaped configuration, when the neutron is about between the two α-particles: $r = 3.5$ fm, $R = 0.5$ fm. However the contribution of this configuration is small and there is a large probability of realization of the configurations at $(r, R) = (3.5, 3.2)$ fm (triangle) or $(r, R) = (3.5, 10.0)$ fm (halo).

One can see another picture in Figure 2, where the three-dimensional profile of wave function of the excited $J^\pi = 5/2^-$ state is shown. With AB potential the function inside the nucleus ($r \leq 1.0$ fm) equals zero, has one maximum at $(r, R) \approx (2.5, 5.5)$ fm, and asymptotically approaches zero at $(r, R) \approx (4.0, 5.0)$ fm. In Buck potential the function is totally located in the inner part of the nucleus with the maximum at $(r, R) \approx (0.7, 1.5)$ fm, its asymptotic is less extended and ends at $(r, R) \approx (2.0, 4.5)$ fm. In both models

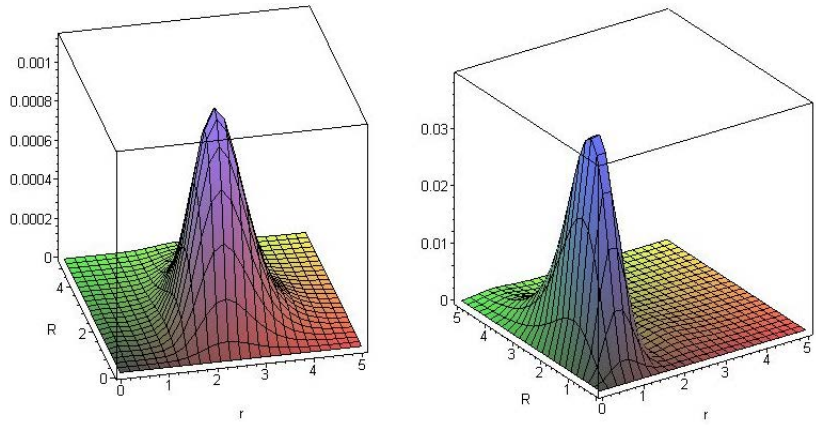

Figure 2. Three-dimensional profiles of ^{9}Be nucleus wave functions in the excited $J^\pi = 5/2^-$ state with AB (left) and Buck (right) potentials

one observes the extremely compact distribution of nucleons with clusters wave functions overlapping.

The explanation of the different behavior of the wave functions in $3/2^+$ and $5/2^-$ states is in the shell structure of the ^{9}Be nucleus. In the $3/2^+$ state the valence nucleon fills the $(2s-2d)$ shell, and that increases the radius of the nucleus and defines its halo-structure; in $5/2^-$ state the nucleon remains on $1p$-shell and the radius does not increase. This agrees with the calculation of the mean-square radii: $\langle r^2\rangle^{1/2} = 2.976$ fm for the $J^\pi = 3/2^+$ state and $\langle r^2\rangle^{1/2} = 2.13$ fm for the $J^\pi = 5/2^-$ state.

Thus, for the excited states of the ^{9}Be nucleus one observes the different pictures: for the $J^\pi = 3/2^+$ state the extended neutron distribution defining its diffuse structure, and for the $J^\pi = 5/2^-$ state the compact one with cluster overlapping in the inner part of the nucleus.

4 Results Analysis

In Figures 3 and 4 there are calculations of the differential cross section of the inelastic p^{9}Be-scattering with different model wave functions of the ^{9}Be nucleus. The differential cross sections for the $J^\pi = 3/2^+, 5/2^-$ states with which authors compare their calculations have been measured in an experiment carried out at the cyclotron laboratory of Indiana University [9] at $E_p = 180$ MeV.

In Figure 3 (scattering for the $J^\pi = 3/2^+$ level) it is seen that the differential cross section with three-particle wave functions in the part of forward angles ($\theta \prec 40^\circ$) coincides well with the experiment, however at angle increase the calculation goes lower than the experimental data. The minimum in the differential cross section at $\theta \to 0^\circ$ is caused by the orthogonality of the wave functions of the initial and final states of the ^{9}Be nucleus. Further the cross section in-

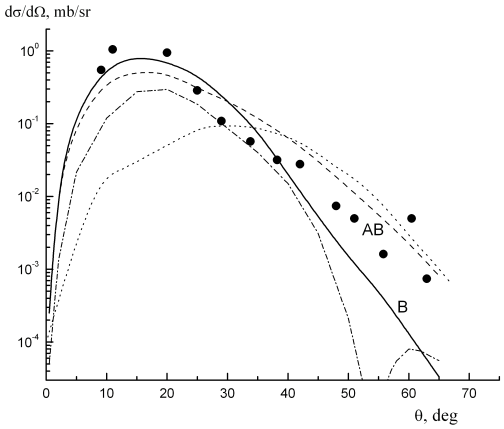

Figure 3. Differential cross sections of inelastic p^9Be-scattering for the $J^\pi = 3/2^+$ level with different model wave functions of the ^{9}Be nucleus. The solid (model 2) and dashed (model 1) curves, dash-dotted curve - with oscillatory wave function, dotted - from paper [9].

creases rapidly until the maximum, and after it decreases monotonically as the scattering angle increases. The contribution to the differential cross sections at small angles depends on the behavior of the wave function at asymptotic. As the abovementioned analysis of the profiles shows, the wave function calculated in the model 1 has the r-coordinate extended asymptotic (extending until ~ 9 fm) and the much more R-coordinate extended asymptotic (extending until ~ 18 fm) what leads to a rapid increase of the cross section at small angles. The maximum of the calculated differential cross section is close to the maximum of the experimental one; however at $\theta \succ 40^\circ$ it decreases more rapidly than the experimental one where the inner part of the nucleus influences. The cross section with the shell wave function $\Psi_f = 1d_{3/2}$ correlates less well with the experimental data in all angle range.

For comparison the authors show the result of differential cross section calculation (dotted curve) in the distorted wave approximation with the effective interaction dependent on the density and based on the Paris potential with the shell wave function [9]. However this curve describes less well the experiment: its maximum is shifted for 20° to the large angles and the value of the cross section is essentially less for small angles (momentum transfer) and essentially more for large angles.

Note that the Glauber theory has essential restrictions for energy and angle range of the particles scattered. Since the incident particles energy is not too large, then the results are reliable for forward scattering angles only. The calculation at large angles is beyond the Glauber theory accuracy.

In Figure 4 there is a calculation of the differential cross section for the

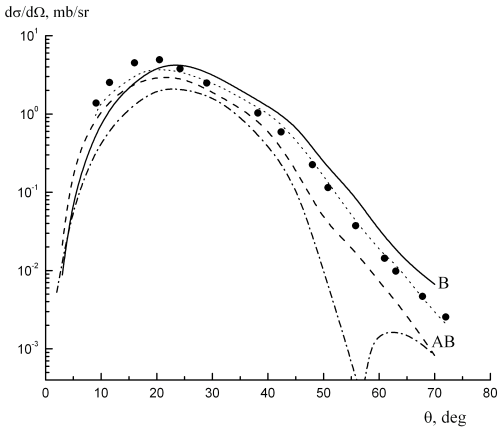

Figure 4. The same as in Figure 3 for the $J^\pi = 5/2^-$ level.

$J^\pi = 5/2^-$ level. The calculation is carried out with two model wave functions. As it is seen from Figure 2, the wave function in the model 1 due to the repulsive core in the inner part of the nucleus disappears, its maximum is located at $(r, R) = (2.5, 1.5)$ fm, and it decreases until zero at $(r, R) = (4.5, 5.5)$ fm. The wave function in the model 2 is strongly involved into the inner part of the nucleus, its asymptotic extends until $(r, R) = (2.0, 5.0)$ fm only. That is why at small angles (where the main contribution is given by the asymptotic of the wave function) the differential cross sections in the model 2 and in the oscillatory one increase slowly and do not reach the maximum of the experimental values. In the inner part the wave function in the model 2 is more compact $(r, R) = (0.5, 1.5)$ fm, and in the model 1 is more extended $(r, R) = (2.5, 2.0)$ fm, what reflects the behavior of the cross sections in the range of large angles ($\theta \succ 30^\circ$). Note that the calculation describes badly the experimental data (all curves lie higher or lower than the experimental values). Here for comparison the authors show the result of the differential cross section calculation (dotted curve) in the distorted wave approximation from paper [9]. It is seen that the calculation of the differential cross section for the level of the negative parity $J^\pi = 5/2^-$ agrees completely with the experiment, while the differential cross section for the level of the positive parity (Figure 3), in opposite, differs from the experiment enough strongly.

5 Conclusion

The authors calculated the differential cross sections of the inelastic p^9Be-scattering for the $J^\pi = 3/2^+, 5/2^-$ levels at proton energies of 180 MeV and compared them with the experimental data and with the calculation in the distorted waves method [9]. The agreement with the experimental data for the $3/2^-$ level is in

the range of forward $\theta < 40^0$ angles, while for the $5/2^-$ level all curves calculated go lower or higher than the experiment. The analysis of the profiles of the wave functions in 2αn-models showed that in the excited $J^\pi = 3/2^+, 5/2^-$ states the nucleus has different structures: diffuse with extended asymptotic (with long tail) in the $3/2^+$ state and compact with short asymptotic in the $5/2^-$ state. The calculation of the mean-square radii confirms this conclusion: 2.976 fm for the $J^\pi = 3/2^+$ state and 2.13 fm for the $J^\pi = 5/2^-$ state. The wave function in the model 1 (for the $3/2^+$ state) inside the nucleus equals zero and reaches the maximal value at $r \approx 3.3 - 3.5$ fm and asymptotically decrease until zero at $r \approx 18$ fm. The wave functions in the model 1 and 2 (for the $5/2^-$ state) are localized in the inner part of the nucleus: the maximum of the first one is located near the centre of the nucleus; the maximum of the second one is distant from the centre for 2 fm. And at that the functions decrease rapidly and go for asymptotic yet at $(r, R) = (4.5, 5.0)$ fm.

The analysis of the wave functions allowed one to connect them with the behavior of the cross sections and show the influence of the contribution of the wave functions different parts on the differential cross sections. The curves calculated with various interaction potentials describe the experimental data differently. The best description of the differential cross sections for the level $3/2^+$ at small angles is observed in the model 2. While for the $5/2^-$ level it is described badly in both the models, and that shows the inadequate choice or calculation of the wave functions for the levels of negative parity.

Acknowledgements

This investigation was financially supported by the Ministry of Education and Science of the Republic of Kazakhstan, grant 3094/GF4.

References

[1] D.R. Tilley, J.N. Kelley, J.L. Godwin *et al*, *Nucl. Phys. A.* **745** (2004) 155.

[2] M. Freer, *Rep. Prof. Phys.* **70** (2004) 2149.

[3] N. Keeley, N. Alamanos, K. Rusek and K.W. Kemper, *Phys. Rev. C* **71** (2005) 014611.

[4] S.K. Pandit, V. Jha, K. Mahata S.Santra et al., *Phys. Rev. C* **84** (2011) 031601(R).

[5] W. Zahn, *Nucl. Phys. A* **138** (1976) 269.

[6] E. Garrido, D.V. Fedorov and A.S. Jensen, *Phys. Lett. B* **132** (2010) 684.

[7] R. Alvarez-Rodrigues, H.O.U. Fynbo, A.S. Jensen and E. Garrido, *Phys. Rev. Lett.* **100** (2008) 192501.

[8] G. Roy et al., *Nucl. Phys. A* **686** (1985) 442.

[9] S. Dixit, W. Bertozzi, T.N. Butti et al., *Phys. Rev. C* **43** (1991) 1758.

[10] S.M. Lukyanov, A.S. Denikin, E.I. Voskoboynik et al., arXiv:1310.2965v3 nucl-ex

[11] A.A. Ogloblin, A.N. Danilov, T.L. Belyaeva et al., *Phys. Rev. C* **84** (2011) 054611; *Int. J. Modern Phys. E* **20** (2011) 823.

[12] E.T. Ibraeva, M.A. Zhusupov, *Phys. Part. Nucl.* **31** (2000) 1359; E.T. Ibraeva, M.A. Zhusupov, A.Yu. Zaykin and Sh.Sh. Sagindykov, *Phys. Atom. Nucl.* **72** (2009) 1773.

[13] E.T. Ibraeva, M.A. Zhusupov, A.V. Dzhazairov-Kakhramanov, P.M. Krassovitskiy, *Nucl. Phys. A* **933** (2015) 16.

[14] M.A. Zhusupov, E.T. Ibraeva, P.M. Krassovitskiy, *Phys. Atom. Nucl.* **78** (2015) 156.

[15] R.G. Glauber, "*High-Energy Collision Theory*", Lectures in Theoretical. Physics, Vol. I, ed. W. E. Brittin et al. (Interscience, New York, 1959).

[16] V.T. Voronchev, V.I. Kukulin, V.N. Pomerantsev, *Few-Body Systems* **18** (1995) 191.

[17] V.I. Kukulin, V.N. Pomerantsev, Kh.D. Rasikov et al., *Nucl. Phys. A.* **586** (1995) 151.

[18] D.A. Varshalovich, A.N. Moskalev, V.K. Khersonskiy, "*Kvantovaya teoriya uglovogo momenta*" (Nauka, Moscow, 1975).

[19] S. Ali, A.R. Bodmer, *Nucl. Phys.* **80** (1966) 99.

[20] B. Buck, H. Friedrich, C. Wheatley, *Nucl. Phys. A* **275** (1977) 246.